TERRA: Terrain Extraction from elevation Rasters 6 through Repetitive Anisotropic filtering 7 8 9

Anton Pijl, Jean-Stéphane Bailly, Denis Feurer, Mohamed Amine El Maaoui, Mohamed Rached Boussema, Paolo Tarolli

TERRA: Terrain Extraction from elevation Rasters through Repetitive Anisotropic filtering

Anton Pijl* [a]; Jean-Stéphane Bailly [b, c]; Denis Feurer [b]; Mohamed Amine El Maaoui [d]; Mohamed Rached Boussema [d]; Paolo Tarolli [a]

[a] Dept. of Land, Environment, Agriculture and Forestry, University of Padova, 35020 Legnaro (PD), Italy (* anton.pijl@phd.unipd.it; paolo.tarolli@unipd.it)

[b] LISAH, University of Montpellier, INRA, IRD, Montpellier SupAgro, Montpellier, France (denis.feurer@ird.fr)

[c] AgroParisTech, 75231 Paris, France (bailly@agroparistech.fr)

[d] ENIT, 1002 Tunis, Tunisia (maaouiamine@yahoo.fr; rached.boussema@enit.rnu.tn)

ABSTRACT

Over the past decades, several filters have been developed to derive a Digital Terrain Model (DTM) from a Digital Surface Model (DSM), by means of filtering out aboveground objects such as vegetation. In this filtering process, however, one of the major challenges remains to precisely distinguish sharp terrain features, e.g. ridges, agricultural terraces or other anthropogenic geomorphology such as open-pit mines, riverbanks or road ramps. Hence, loss of elevation data around terrain edges (and consequent smoothing) is very common with existing algorithms. In terraced landscapes, the preservation of precise geomorphology is of key importance in digital terrain analyses, such as hydrologic and erosion modelling, or automatic feature recognition and inventorying. In this work, we propose a new filtering method called TERRA (Terrain Extraction from elevation Rasters through Repetitive Anisotropic filtering). The novelty of the algorithm lies within its usage of terrain aspect to guide the anisotropic filtering direction, therefore maximising the preservation of terrain edges. We derived six DTMs from DSMs using UAV Structure from Motion (SfM) photogrammetry, laser altimetry and satellite sources (grid resolutions ranging from 0.1−1.0 m). The results indicated a close agreement of DTMs filtered using the TERRA algorithm and reference DTMs, while terrace risers were well preserved even under thick canopies of vines and trees. Compared to existing filtering approaches, TERRA performed well in minimising Type I errors (false ground removal), while Type II errors occurred locally where vegetation was covering the terrace edges. Given the promising filtering performance, and supported by the minimal requirements of parameterisation and computation, the TERRA algorithm could be a useful tool in DTM preparation for digital terrain analysis of agricultural terraces and similar hillslopes characterised by a complex mosaic of sharp terrain and non-terrain features.

Keywords: Digital Terrain Model (DTM) extraction; terraces; anisotropic filtering; vegetation removal; edge preservation

Graphical abstract

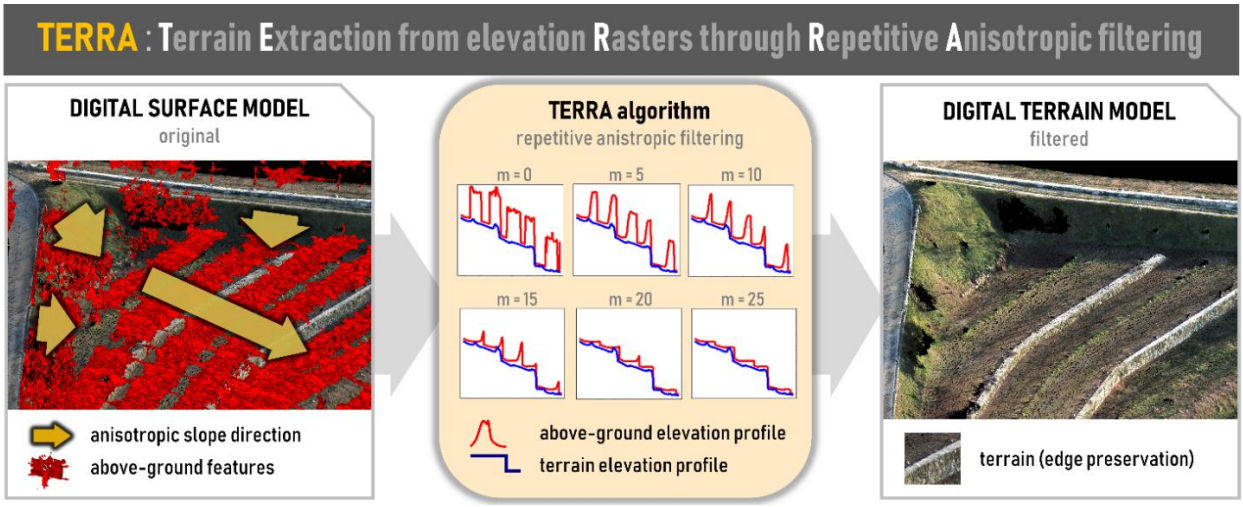

1. INTRODUCTION

Topographic data are widely used as powerful supportive information in various fields of research and in civil applications, such as environmental management or landscape planning. With modern advances in remote sensing techniques, such data are increasingly accessible with improving level of detail (Passalacqua et al., 2015; Tarolli, 2014), often organised as regular-grid Digital Elevation Models (DEMs). Remotely sensed elevation data, however, typically contains both bare-earth and aboveground information such as vegetation cover (Digital Surface Model, DSM). Many

applications require either purely ground information (Digital Terrain Model, DTM), e.g. in hydrology, or the height difference of a DTM and DSM, e.g. as a Canopy Height Model (CHM). Therefore, differentiation between ground and non-ground elevation data is of wide interest. A range of systematic filtering methods have thus emerged, which however have a common issue with the preservation of sharp terrain features (Liu, 2008; Meng et al., 2010). This limits reliable digital terrain analysis in landscapes characterised by terrain ridges, or sharp anthropogenic features such as open-pit mines, riverbanks, urban ramps or agricultural terraces. Terraced landscapes represent one of the most widespread examples of complex anthropogenic geomorphology (Tarolli et al., 2014; Wei et al., 2016), of which the culture-historical and economic values are widely recognised, e.g. by the United Nations Educational, Scientific and Cultural Organization (UNESCO) and the Food and Agriculture Organization (FAO) (Dela-Cruz and Koohafkan, 2009). Precise information on terrain morphology is of key importance in several types of terrace terrain analysis, e.g. (semi-)automatic terrace recognition and inventories (Bailly and Levavasseur, 2012; Sofia et al., 2016, 2014), high-precision soil erosion simulations (Pijl et al., 2019a; Tarolli et al., 2015) or digital designs of terrace drainage systems (Pijl et al., 2019b).

Various approaches exist for identifying terrain from regular-grid DSM, that are typically based on geometrical characteristics such as slope (Roggero, 2001; Sithole, 2001; Vosselman, 2000), mathematical morphology (Chen et al., 2007; Zhang et al., 2003), or alternatively on linear prediction or interpolation-based methods (Kraus and Pfeifer, 1998). In order to provide a systematic comparison of ground-filtering algorithms, the ISPRS Working Group III/3 evaluated the performance of eight established methods (Sithole and Vosselman, 2004). These algorithms (developed by Axelsson, 1999; Brovelli et al., 2002; Elmqvist et al., 2001; Pfeifer et al., 1998; Roggero, 2001; Sithole, 2001; Sohn and Dowman, 2002; Wack and Wimmer, 2002) represented the different filtering approaches and were tested for different landscape types and elements. Three terrain types were found to be particularly challenging: steep slopes, vegetated slopes, and discontinuous terrain features. Interestingly, all three characteristics are typical descriptors of terraced landscapes, making it one of the most challenging environments for automatic DTM-from-DSM generation. Under these circumstances, typically, ground features are falsely removed as aboveground features (Type I error). In particular, sharp ridges were shown to be very poorly preserved, with 7 of 8 algorithms removing these elements in >50 % of all cases, and 1 algorithm in 10−50 % of cases (Sithole and Vosselman, 2004).

The difficulties of filtering discontinuous terrain are pointed out by Meng et al. (2010) as well, who relate it to the conventional assumptions about (non-)terrain geometry that underlie the algorithms. Sharp geomorphological features share 3 out of 4 typical properties of non-ground features, i.e. steep slopes, large elevation differences, and local heterogeneity of elevations. The edge-preservation challenge is widely reported in diverse filtering approaches, e.g. multi-directional ground filtering (Meng et al., 2009), one-dimensional and bi-directional labelling (Shan and Aparajithan, 2005), or Simple Morphological Filter aided by novel image-processing techniques (Pingel et al., 2013). The two-step adaptive extraction method by Yang et al. (2016), specifically designed to preserve terrain breaklines, also produces Type I errors (false ground-point removal) around terrace edges, underlining the persisting challenges of this terrain type. An increasingly common approach is segmentation-based filtering based on supervised training (Grilli et al., 2017). Famous examples include graph-cut methods (He et al., 2018; Ural and Shan, 2016) or the CANUPO algorithm (Brodu and Lague, 2012), which group data points based on multi-scale homogeneity in geometric characteristics. Despite their powerful potential in many applications, such approaches rely on active supervised learning and are known to be computationally very heavy, both limiting their adoption and suitability for large-scale analyses (Grilli et al., 2017; Lermé and Malgouyres, 2017). Also non-geomorphologic filters reportedly have limited applicability in these terraced landscapes, e.g. NDVI-

based segmentation in vineyard terraces that is typically hampered by grass cover (Burgos et al., 2015; Santesteban et al., 2013).

Interesting opportunities, however, lie in the regular geometry of hillslope terrain, particularly in engineered terraces. Anisotropic filtering holds potential for terrain edge-preservation in the filtering process (Passalacqua et al., 2015). Given that slope aspect is often not entirely mono-directional across hillslopes, its local anisotropy could dictate the filtering direction. While anisotropy or non-linear filters has been successfully applied for edge-preserving terrain smoothing from noise (Passalacqua et al., 2015; Perona and Malik, 1990), a filter driven from terrain slope anisotropy has not been developed before, to the best of our knowledge. If one can assume that ground elevation changes are locally homogeneous in sign (i.e. consistently up- or downhill), a simple iterative erosive operation could progressively remove objects with opposite elevation change.

This paper proposes a novel DTM-from-DSM filtering algorithm called TERRA (Terrain Extraction from elevation Rasters through Repetitive Anisotropic filtering). The filter has a primary focus on the preservation of sharp terrain features on complex vegetated hillslopes, by acting as an anisotropic erosive terrain "scrapper" whilst maintaining larger perpendicular objects such as contour terraces. The regular-grid approach of the TERRA algorithm favours its time-efficiency (Grilli et al., 2017; Shan and Aparajithan, 2005; Wack and Wimmer, 2002) and allows generic applicability, i.e. it could be applied independently of data source and surveying platform. Thus, the algorithm could be a powerful tool in DTM creation e.g. in support of high-resolution analysis on field scale (e.g. LiDAR- or photogrammetry-based) or large-scale geomorphologic inventories (e.g. satellite-based). Filtering performance is evaluated in terms of non-ground removal and ground preservation compared to ground-truth elevation data, as tested on six different topographic datasets of challenging vegetated terrace landscapes.

Section 2 of this article elaborates on the technical details of the TERRA algorithm (2.1), the background of the several test sites (2.2), the diverse origin of topographic data (2.3), the parameterisation of the algorithm (2.4), and the experimental design for performance assessment of TERRA (2.5). Filtering results by TERRA and its performance are then presented in Section 3, while Section 4 furthermore touches on its limitations and further potential.

2. MATERIALS AND METHODS

2.1 TERRA: a new digital elevation model filtering algorithm

The TERRA algorithm virtually acts as a "scrapper" removing topsoil elements in the slope direction at each DSM grid node. It works as a smoothing operation but locally directed along the slope while only considering downhill neighbouring values. Firstly, it computes the slope direction (aspect) at coarser spatial resolution as a multiplication of aggregation factor η and grid resolution r, thus avoiding slope noising resulting from vegetation and preventing interruption by non-terrain features. This slope direction is secondly resampled at each initial DSM grid node (Figure 1, note that the aggregation window for determining slope direction is kept relatively small in this figure for visual understanding). TERRA then operates as an iterative focal anisotropic filter. For each grid node (i,j) of the DSM at a given iteration m, anisotropy results from null weights given by kernel function K to downstream nodes within the focal window, i.e. in front of the semi-circular sector of the slope aspect at (i,j) node (Figure 1).

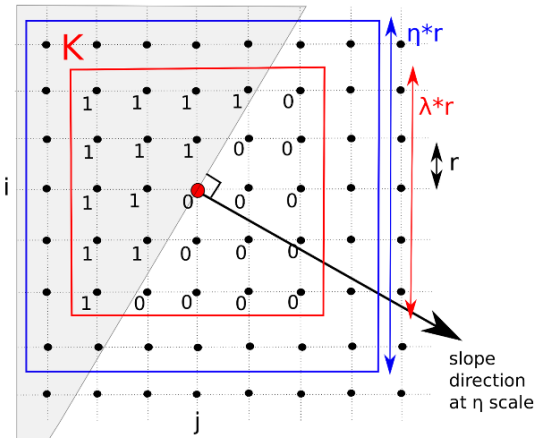

Figure 1 – Schematic top-view of the TERRA filtering algorithm, showing the determination of hillslope aspect (coarser resolution with η cells) and subsequent attribution of null weights to all downstream grid nodes within kernel K (finer resolution with λ cells).

At each iteration *m* over the grid, elevation value Z_m on grid node *(i,j)* is computed as:

$$Z_m(i,j) = argmin(Z_{m-1}(i,j),\ K_{i,j}(\lambda,\eta)) \quad \text{(Eq.1)}$$

With $K_{i,j}(\lambda,\eta)$ as the chosen kernel averaging function (e.g. median). The processes is repeated from *m* equal to 1 up to *M*, the total number of iterations. The three algorithm parameters *η, M* and *λ* can be linked to physical properties of the studied surface. Let us consider the terrain features of interest are of maximum size *c*r* and topsoil elements to remove are of maximum length *b*r* along slope direction (illustrated in Figure 2, corresponding to the study case in Figure 3, bottom-right). According to the Nyquist-Shannon theorem of sampling, the *η* parameter should be chosen in order to preserve terrain contour curvature at least two times coarser than *c* (*η >= 2c*). The *M* parameter should be initiated with the value of *b*, given that the iterative filtering will "scrap" a given non-terrain object cell by cell, with a maximum number of *b* (this iterative filtering is illustrated in Figure 2). The latter *λ* parameter is less sensitive and controls the desired level of smoothing on terrain data related to the used kernel averaging function. The TERRA algorithm is freely available as R script under GNU GPL licence at: https://www.umr-lisah.fr/?q=fr/scriptsr/terra-script-r (see Supplementary Material A).

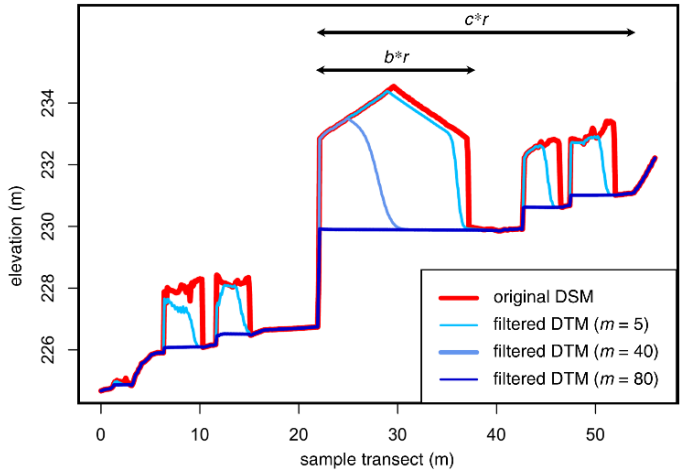

*Figure 2 – Schematic side-view transect elevation profile of a DSM and several DTMs filtered with given iterations m, illustrating also the physical meaning of b*r (maximum downslope length of non-terrain object) and c*r (dimension of typical terrain features, here a terrace bank). The determination of slope direction at η-scale (i.e. right-to-left direction) is not affected by local interruptions such as the building or vegetation, considering that η >= 2c.*

2.2 Test sites

A total of four test sites across three Mediterranean countries were used for testing the TERRA algorithm (Figure 3). These locations provided six distinct application scenarios due to multiple topographic data sources in some of the sites (Table 1). A common characteristic of all sites is the presence of agricultural terraces that are to some extent covered by vegetation. In Italy, two terraced vineyards are selected that are characterised by dry-stone walls (vertical) and earth banks (typically inclined to about 45°), respectively located in the Verona province (45°31'36.80"N; 10°54'54.32"E) and Treviso province (45°56'43.26"N; 12°10'4.49"E). The Roujan site is part of an observatory in Mediterranean France (43°28'56.01"N; 3°20'55.69"E) that has been monitored since 1992 (ORE OMERE: http://www.obs-omere.org/; Molénat et al., 2018), containing wider vineyard terraces with intermittent dry-stone walls that are partly covered in natural shrubs. The Cap Bon test site in Tunisia (36°52'55.68"N; 10°54'45.25"E) is located on the steep slopes of a hill where a mixed soil conservation system was settled. This soil conservation system consists in small shrubs associated to contour lines benches. This test site is located just near to Kamech, the second site of the OMERE observatory mentioned above.

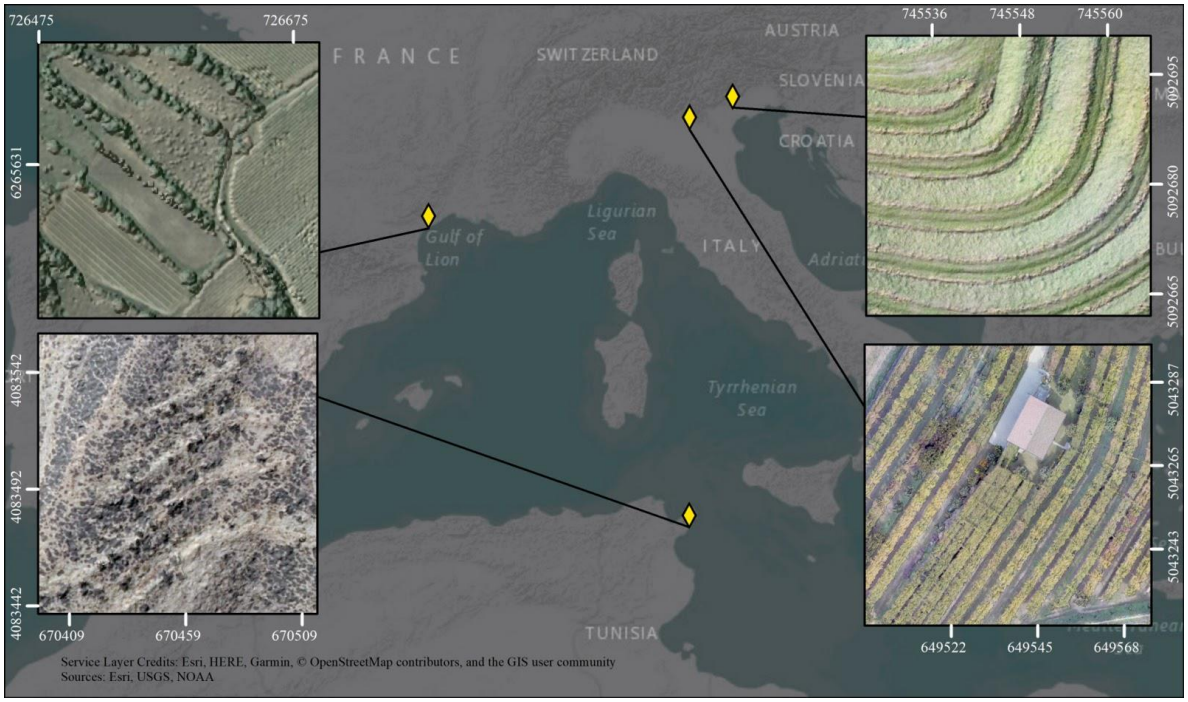

Figure 3 – Location of the four test sites of this study: Roujan, France (top-left); Kamech, Tunisia (bottom-left); Treviso, Italy (top-right); and Verona, Italy (bottom-right). For each site, orthomosaics are displayed with geographical extent in the WGS 84-UTM 32 coordinate system (EPSG:32632).

2.3 Topographic data sources

The various sites offer an interesting set of test cases, given their diversity in topographic data source. In Treviso (TRE) and Verona sites (VER-O and VER-D), very high-resolution elevation data (0.1 m) was obtained using Unmanned Aerial Vehicles (UAVs) and photogrammetric processing. An independent source of ground elevation data was provided through accurate field-measurements of DGPS reference points. In Roujan, high-resolution surface topography data (1 m) was obtained from Pleiades optical satellite imagery (ROU-P) and LiDAR laser altimetry (ROU-L), with the latter also providing a reference terrain model without vegetation. The Kamech dataset (KAM), high-resolution elevation data (0.3 m) was obtained by photogrammetric processing of digital aerial imagery acquired by the Tunisian office of topography and cadastre.

166 *UAV-SfM photogrammetry*

167 In Treviso and Verona, UAV surveys were carried out during October 2017 (TRE and VER-O datasets) using a *DJI*
168 *Phantom 4 Pro* (20 MP optical camera with 8.8 mm focal length). In the latter site, a repeated UAV survey was carried
169 out during December 2017 (VER-D dataset), when no leaves were present on the grape vines, using a *DJI Mavic Pro*
170 (12.3 MP optical camera with 4.7 mm focal length). Nadir images were taken from a 50-m altitude with >75 % front- and
171 side-overlap, and oblique images were sparsely captured to better cover hidden parts (e.g. terrace fronts or vegetation
172 blind spots), with a total number of 316, 146 and 254 images for TRE, VER-O and VER-D, respectively. Reference
173 terrain elevation points were measured using a *TopCon HyperV* DGPS device for calibration of the photogrammetric
174 analysis (resp. 18, 19 and 17 ground control points) and as an independent validation dataset for the vegetation filtering
175 process (dense transects of 60 and 200 points for the two locations, resp.).

176 UAV imagery was processed using Structure-from-Motion (SfM) photogrammetry software *Agisoft Photoscan*, in order
177 to derive a 3D model from the overlapping 2D images and additional ground control points. The resulting dense point
178 clouds had a point density of 694, 1545 and 2023 pt/m² and a recommended DEM resolution of 0.03, 0.02 and 0.02 m/pix,
179 which was harmonised to 0.1 m for the TRE, VER-O and VER-D datasets. In addition to the DSMs, reference DTMs
180 were derived by manual point cloud filtering (further elaborated in Section 2.5), with vertical errors to DGPS points of
181 0.09±0.06 m, 0.02±0.06 m and 0.02±0.10 m, respectively for the three datasets.

182 *Table 1 – Study sites and their main characteristics, used in this study for testing the filtering algorithm.*

DATASET ACRONYM	LOCATION	TERRACE TYPE	VEGETATION TYPE	DATA SOURCE	REFERENCE DTM	RESOLUTION (m)
TRE	Treviso (IT)	earth banks, relatively steep	vineyards (rows)	UAV SfM	manual filtering + DGPS	0.1
VER-O	Verona (IT)	earth banks & dry-stone walls	vineyards (pergola cultivation), leaves-on	UAV SfM	manual filtering (VER-D) + DGPS	0.1
VER-D	"	"	vineyards (pergola cultivation), no leaves	UAV SfM	manual filtering + DGPS	0.1
ROU-L	Roujan (FR)	dry-stone walls, partly vegetated	vineyards (rows), lines of trees and bushes	LiDAR	LiDAR DTM	1.0
ROU-P	"	"	"	Pleiades (stereoscopic)	LiDAR DTM (ROU-L)	1.0
KAM	Kamech (TN)	contour bunds	sparse trees and low bush	aircraft SfM	manual filtering	0.3

183
184

Multi-echo LiDAR

In Roujan, Aerial Laser Scanning (ALS) was carried out during June 2002. A helicopter mounted with a *Falcon II Toposys* LiDAR system covered the area from a 900-m altitude, with a 83 MHz laser pulse emission rate and a 10 pt/m² 3D points spatial sampling rate. Multi-echo information was used to create a 1-m DSM (from first pulse points) and DTM (from last pulse points, followed by a multi-step filtering process). For more details about this particular ALS survey and data processing, the authors refer to Bailly et al. (2008). DGPS validation points taken in the field showed a vertical error standard deviation of the 1-m DTM of 0.06 m in flat areas and 0.15 m on the steepest slopes.

Pleiades satellite

In Roujan, Pleiades satellite imagery was recorded during the leaves-off period of January 2013 (ROU-P). A stereo pair of images was taken with a high incident angle of 30° (base-to-height ratio of about 1/1.6). A 1-m DSM was constructed using *MICMAC* software (Pierrot-Deseilligny et al., 2011; Pierrot-Deseilligny and Paparoditis, 2006). For more technical details on the photogrammetric analysis of this particular dataset, the authors refer to Sofia et al. (2016). Validation with ground-measured DGPS points showed a vertical error standard deviation of 0.51 m.

Airborne SfM photogrammetry

For Kamech (KAM), aerial imagery was available from airborne survey performed by the Tunisian office of topography and cadastre during June 2010. The whole set of images was acquired with a *Vexcel UltraCamXp* at an average altitude of 5200 m. From this set, four images covering the area of interest were extracted. Each image has 11310*17310 pixels with an average ground sampling distance of 0.3 m. Four GCPs picked on Google Earth imagery were used to obtain an absolute geographic reference (estimated vertical accuracy <10 m). SfM photogrammetric processing was carried out using *Agisoft Photoscan* software and a DEM at 0.3 m resolution was exported. For this test site, no validation data is available.

2.4 Parameterisation

The TERRA algorithm was tested for the six test datasets with the parameters given in Table 2. Aspect aggregation factor η and number of iterations M were determined from the physical dimensions of area-specific objects. Both parameters should be at least the downslope length of non-terrain objects: for η to correctly determine terrain aspect, and for M to allow enough "scrapping" iterations to remove the object (as described in Section 2.1). Parameter values could be translated into metric equivalents by considering raster resolutions (see Table 1), e.g. if the *pergola* canopy found in VER-D has a maximum downhill length of 8 m, the η and M parameters could be set to 100 (10 m equivalent * 0.1 m resolution). Finally, kernel size (λ) was set to 7 for all datasets, based on an arbitrary assumption of allowed semi-circular (downhill) smoothing. Initial tests suggested limited sensitivity of the produced results by varying kernel sizes, although no elaborate sensitivity analysis was carried out for this parameter in the presented study.

Table 2 – TERRA parameter values used in this study.

DATASET	ASPECT AGGREGATION FACTOR (η)	TOTAL NUMBER ITERATIONS (M)	KERNEL SIZE (λ)
TRE	**30** (equiv. 3 m)	**30** (equiv. 3 m)	7
VER-O	**100** (equiv. 10 m)	**100** (equiv. 10 m)	7
VER-D	**100** (equiv. 10 m)	**100** (equiv. 10 m)	7
ROU-L	**30** (equiv. 30 m)	**30** (equiv. 30 m)	7
ROU-P	**30** (equiv. 30 m)	**30** (equiv. 30 m)	7
KAM	**30** (equiv. 9 m)	**30** (equiv. 9 m)	7

2.5 Reference DTMs and filtering performance assessment

Reference DTMs were available from different sources varying among datasets (Table 1). For the SfM-photogrammetric datasets (i.e. TRE, VER-O, VER-D, KAM), a reference terrain model was obtained by manual filtering based on the original point cloud, which is an established approach for relatively small datasets (Meng et al., 2010; Sithole and Vosselman, 2004). The manual filtering was done using *CloudCompare v2.9.1* software, based on the vertical distance of any point to surrounding points while paying close attention to the preservation of complex landscape features (examples in Figure 4). An exceptional case was the VER-O dataset, in which ground points were insufficient to provide a complete reference DTM, hence the VER-D reference DTM was used (thus implying an uncertainty due to shifts). For the LiDAR-based dataset ROU-L, a reference DTM was readily available. The same reference DTM was also used for comparison with the filtered ROU-P DTM, after a vertical shift was performed corresponding to the average distance of their DSMs (3.64 m, which relatively homogeneous throughout the study site, with a standard deviation of 0.27 m). Such comparison can further be justified as no changes in terrace morphology were detected between the timing of the ROU-L (2002) and ROU-P (2013) datasets (Sofia et al., 2016), and erosion rates in Roujan are relatively low with a reported 0.695 mm/year (Paroissien et al., 2010).

The filtering performance of TERRA was done in several steps. Firstly, the filtered DTMs were compared to dense DGPS transect available from the field surveys of TRE and VER-O, based on Root Mean Square Error (RSME) values (Section 3.1). Secondly, the filtered DTMs were compared to the original DSMs, based on a visual interpretation of the difference maps (Section 3.2). Lastly, the filtered DTMs were compared to the reference DTMs based on difference maps and transect elevation profiles (Section 3.3). The maps were classified according to Type I and II errors in order to allow a quantitative comparison with literature. For this particular purpose, a threshold was introduced to distinguish between appropriate filtering and terrain underestimation (i.e. false ground removal or Type I error) or overestimation (i.e. false non-ground preservation or Type II error). This threshold was set variable for the different datasets, as twice the raster resolution in case of SfM-derived datasets as empirically estimated in many previous studies (e.g. Lane et al., 2000), thus 0.2 m for TRE, VER-O, VER-D; and 0.6 m for KAM), and as 0.3 m for the ROU-L and ROU-P datasets, corresponding for the former to the 95% confidence band for random altimetric errors in LiDAR measurements.

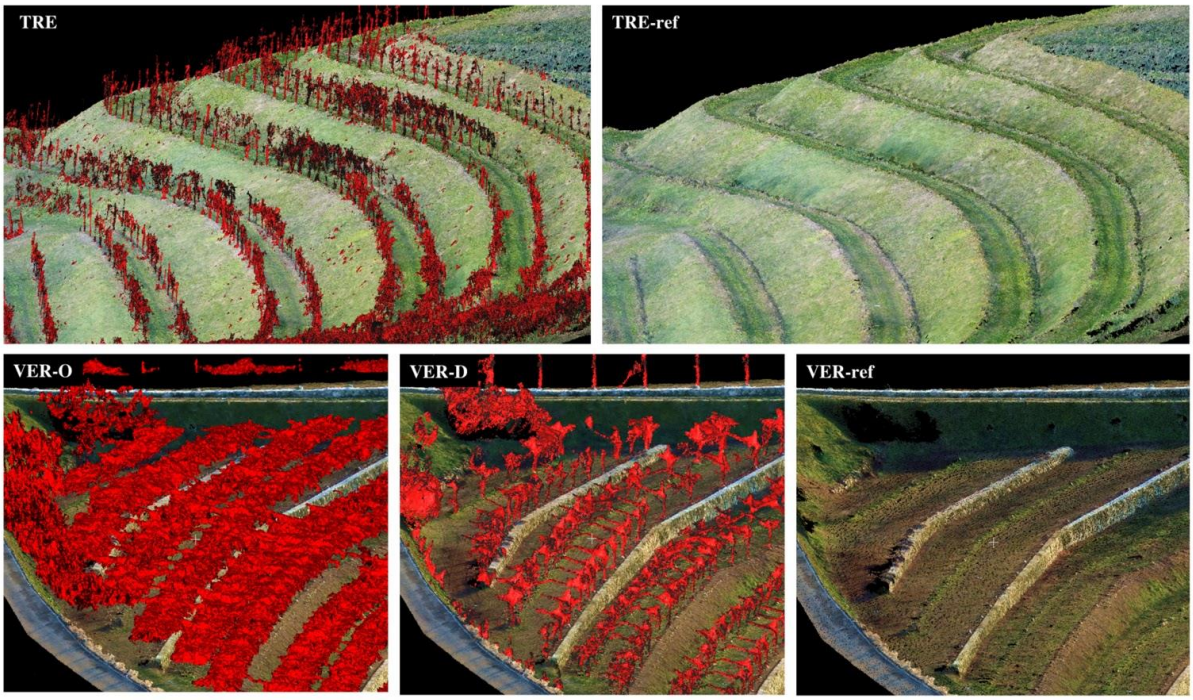

Figure 4 – Snapshot of manual aboveground filtering (red) in preparation of reference DTMs for the VER-O, VER-D and TRE datasets. Various vineyard cultivation types can be distinguished, e.g. the typical pergola in Verona (second row), with a reduction of canopy cover between the UAV flights of October and December, 2017.

3. RESULTS

3.1 Comparison of filtered DTMs and DGPS

Figure 5 illustrates the generally strong agreement between field-measured DGPS points (black circles) and the filtered DTM elevation profile across these points (blue lines) alongside with the original DSM elevations (red lines). RMSE values between the measured points and filtered DTM are respectively 0.121 m and 0.256 m for the TRE and VER-O datasets. In the former, additional comparison of the reference DTM with the DGPS points reveals a RMSE of 0.110 m, indicating that almost the entire error of the filtered DTM can instead be explained by a photogrammetric error (considering also that vegetation is not abundant, see Figure 5). The remaining errors are limited (roughly 0.011 m) and indicate promising filtering performance. This is underlined by the case of VER-O, where thick vegetation coverage is present, and the RMSE of the DSM and DGPS was originally 1.744 m. The remaining error can be attributed to situations where terrace edges are covered in overhanging vegetation, e.g. around VER-O transect lengths 90 m and 170 m in Figure 5. A further comparison of filtered and reference DTMs is given Section 3.3, following a comparison with the original DSMs in Section 3.2.

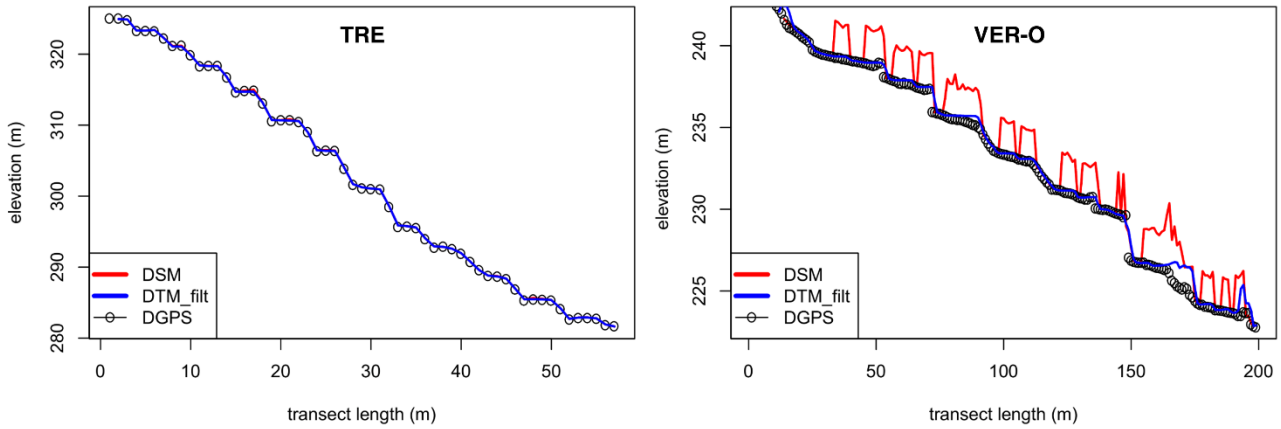

Figure 4 – DGPS transect elevation values (black circles) and corresponding extracts of DSM (red lines) and filtered DTM (blue lines; DTM_filt) in TRE and VER-O datasets.

3.2 Comparison of filtered DTMs and original DSMs

DTMs derived from the original DSMs by the TERRA algorithm are shown in Figure 6 (left and centre columns). The difference maps show clear patterns of aboveground features (right column, reddish colours), such as vine rows (TRE, VER-O, VER-D), the building (VER-O, VER-D), and trees and bushes (VER-D, ROU-L, ROU-P, KAM). Even in VER-O, originally significantly covered in *pergola* type vines, a DTM is derived that is visually very close to VER-D (while the latter has much more ground information). Terrace edges are still evident in VER-O, although additional sharp micro 'ridges' are detectable where the canopy ends on the banks of some terraces (e.g. eastern segment of VER-O, filtered DTM). Some remainders of vegetation can be detected under terrace edges (e.g. middle segments of VER-O and VER-D), which is further explored in the following section. Instead, vegetation located slightly further from ridges are removed well (e.g. visible just north and south of the house in VER-O and VER-D).

3.3 Comparison of filtered and reference DTMs

Difference maps and transect profiles show that there is generally a good agreement between filtered and reference DTMs across the study sites (Figure 7). Sharp terrain edges such as terrace fronts are well preserved throughout the study areas, even in the case of near-vertical stone walls of VER-O and VER-D (Figure 7, e.g. between transect length 90−100 m). Some deviations exist, which are predominantly negative and result from remaining vegetation in the filtered DTM (cyan colours). Two recurring situations of such errors can be recognised:

(i) Dense vegetation is present at the foot of a terrace wall, with elevation values similar to the upslope terrace elevation. In this case, a continuous surface is produced, consisting of terrace terrain elevations and remainders of canopy elevations. Some examples can be found throughout the difference map of VER-D (Figure 7, dashed circles), and related transect at lengths 17 m and 35 m (see dashed arrows).

(ii) Dense vegetation is located on top the terrace and 'overshadowing' the terrace edge. In this case, terrace fronts are estimated to be located at the vegetation edge, which is often too wide compared to the actual bench width. Examples are visible in the transect profiles of VER-O (around 40 m, see dashed arrow), ROU-L and ROU-P (around 25 m and 30 m, see dashed arrows), and throughout the respective difference maps (see dashed circles).

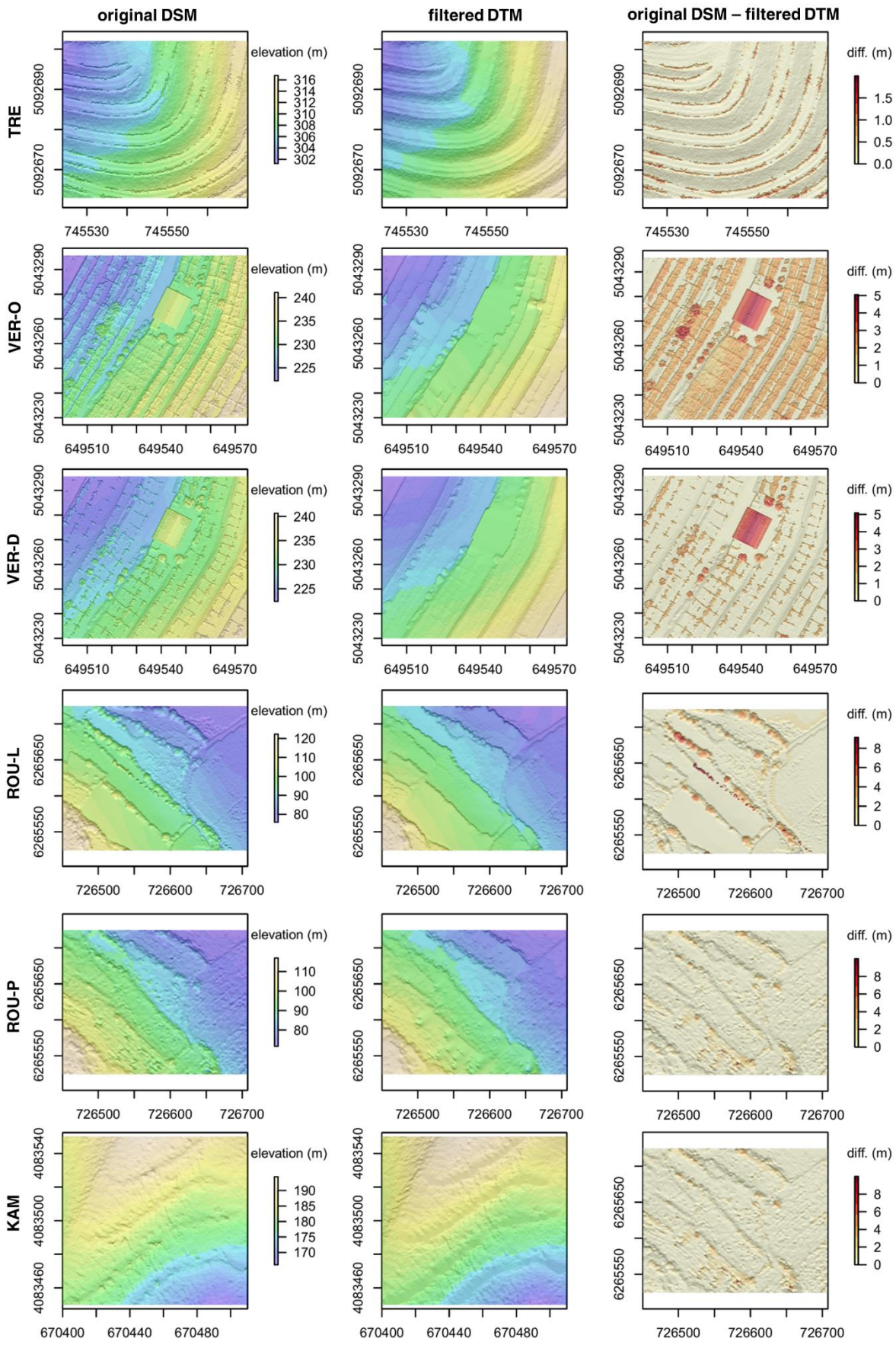

Figure 6 – Digital elevation models for each dataset: the original DSM (left), the DTM filtered using the TERRA algorithm (centre), and the difference map (right); all displayed in coordinate system WGS 84-UTM 32 (EPSG:32632)

A quantification of the spatial distribution of Type I and II errors is provided in Table 3. In general, the TERRA algorithm performs very well in avoiding Type I errors (i.e. ground is preserved), and is more prone to Type II errors (i.e. non-ground is falsely preserved). On average, Type I errors are relatively sparse with 5.1%, which indicates an improved performance compared to the 8 filtering approaches evaluated by Sithole and Vosselman (2004), of which 7 show Type I errors in more than 50% of cases. Type II errors here are generally more frequent with an average of 19.9%, but performance according to Sithole and Vosselman (2004) would be classified as *Fair* (10−50%) or *Good* (<10%) for the individual datasets (Table 3, third column), which is comparable with the 8 considered filters under vegetated slopes. Two datasets show notably high errors: (i) ROU-P in Type I errors occurring on the horizontal terrace banks (Figure 7, ROU-P, purple colours), which can be related to general quality of the dataset combined with the usage of an external reference DTM (from ROU-L); (ii) ROU-L in Type II errors, which are mostly related to a large flat vineyard canopy covering the eastern segment of the study site (Figure 7, ROU-L, cyan colours). Additionally, Type II errors are indeed relatively high in the zones where terrace edges are covered in vegetation (situation –ii– in the previous paragraph), i.e. VER-O (41.2%), ROU-L (18.1%) and ROU-P (50.9%, combined with the effect of the flat vineyard).

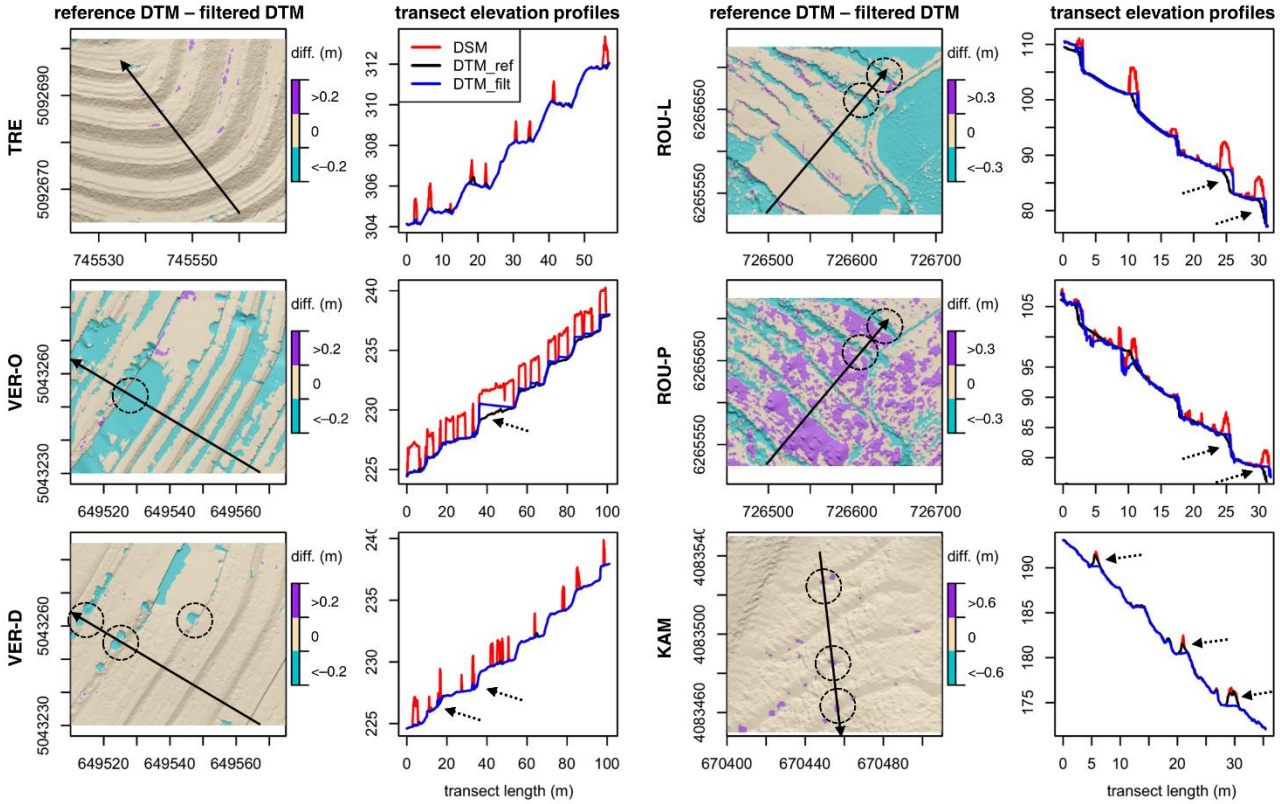

Figure 7 – Distance comparison of terrain elevations: difference maps of reference and filtered DTMs considering a specific threshold for Type I and II errors (resp. purple and cyan colours), and transect elevation values extracted along the black solid arrows depicted on the maps in downhill direction (DSM as red lines; reference DTM as black; filtered DTM as blue); all displayed in coordinate system WGS 84-UTM 32 (EPSG:32632).

Furthermore, the derived DTMs have mean elevations relatively close to the reference DTMs (Table 3), i.e. <10 cm for high-resolution datasets TRE, VER-D and KAM, and <70 cm for the LiDAR-based and Pleiades-based datasets ROU-L and ROU-P. The mean distance between the filtered and reference DTMs of VER-O is slightly higher, which is biased by the different origin of the reference (i.e. deriving from the VER-D survey). Pearson's correlation coefficients of

reference and filtered DTMs range between 0.995 and 0.999 for all datasets, emphasising the expected overall agreement of derived elevation values with the reference on steep slope test sites. Only in the case of KAM the reference DTM is generally higher than the filtered DTM (Table 3), which is related to the slight "scrapping" of the top of the contour bunds (Figure 7, dashed circles and arrows).

Table 3 – Statistics on terrain elevations: mean and standard deviation of the reference DTMs, filtered DTMs, and difference maps; the Pearson correlation coefficient of reference and filtered DTMs; and the Root Mean Square Error (RMSE) of ground-measured DGPS values vs. their extracts from the filtered DTMs.

DATASET	TYPE I errors	TYPE II errors	REFERENCE DTM *mean* ± *std.* (m)	FILTERED DTM *mean* ± *std.* (m)	REFERENCE DTM – FILTERED DTM *mean* ± *std.* (m)	CORRELATION COEFFICIENT *(reference and filtered)*
TRE	1.5%	6.1%	309.21 ± 5.88	309.30 ± 5.83	-0.09 ± 0.59	0.996
VER-O	0.8%	41.2%	229.66 ± 3.73	229.86 ± 3.83	-0.20 ± 0.35	0.995
VER-D	0.8%	3.0%	229.65 ± 3.72	229.65 ± 3.72	0.00 ± 0.11	0.999
ROU-L	3.5%	50.9%	94.2 ± 14.10	94.7 ± 14.20	-0.51 ± 0.81	0.998
ROU-P	23.3%	18.1%	90.6 ± 14.10	91.2 ± 14.20	-0.63 ± 1.07	0.997
KAM	0.9%	0.0%	182.68 ± 6.14	182.68 ± 6.15	0.07 ± 0.11	0.999
average:	*5.1 %*	*19.9 %*	-	-	-	-

4. DISCUSSION

4.1 Performance and novelty of TERRA algorithm

This study presented TERRA, a novel filtering algorithm for deriving a DTM from a DSM. Its development was motivated by the general difficulties that existing filters commonly have with the preservation of sharp terrain features, due to their similarities with non-ground features (Meng et al., 2010, 2009; Pingel et al., 2013; Shan and Aparajithan, 2005). To the best knowledge of the authors, TERRA is the first filter to make use of anisotropy in terrain aspect to guide the filtering direction, and as such, minimise the loss of valuable terrain information (Type I errors).

The studied topographic datasets represent a typical challenge for existing methods, i.e. steep, vegetated and discontinuous slopes (Sithole and Vosselman, 2004), which are all common features of the agricultural terraces considered here. Results show that the TERRA algorithm is able to derive a DTM from a given DSM with terrain elevations very close to the reference (r>0.995), with minimal parameterisation requirements that can easily be estimated *a priori* from the dimensions of known physical objects. The largest deviations from the reference terrain is found where dense vegetation is present around terrace walls, resulting in false preservation of above-ground remainders (Type II errors on 19.9% of surface). However, the TERRA algorithm performs particularly well in preserving terrain features such as terrace edges under diverse conditions of canopy type and the origin of topographic data (Type I errors on 5.1% of surface). The performance is further characterised by relatively fast computations, thanks to the regular-grid data structure, e.g. when compared to 3D point cloud-based filters (Grilli et al., 2017; Lermé and Malgouyres, 2017).

4.2 Limitations of methodology

Limitations to the presented methodologic set-up affect the results due to various reasons, including the algorithm structure and the data origin and comparison. Tests of the TERRA algorithm in various conditions give a good initial confidence of wider application and further testing of the method. The major source of errors in this study is the presence of vegetation around the terrace front, covering the edge either from above or from the side (Section 3.3). Additionally, certain specific topographic conditions could hypothetically to be more difficult in terms of vegetation filtering and terrain preservation:

(i) The presence of contour-structures with risers such as contour bunds or stone walls, that are actually considered part of the terrain but are likely to be "scrapped" (as suggested by the results from the KAM dataset here);

(ii) Highly sinuous hillslopes with strong contour curvature, e.g. in a strongly concave or convex hill segment, will impede the determination of hillside aspect, while the aspect aggregation factor η has a lower limit dictated by the dimensions of non-terrain objects.

Uncertainties in the presented material also result from topographic data sources. Examples include photogrammetric errors or the inherent noise related to satellite stereography, creating artefacts in the DSM. On the one hand, the TERRA filter can cope with this issue, or even improve it by filtering it out. On the other hand, final results will be affected negatively when artefacts are in the dimensional order of magnitude of features of interest (e.g. terrace wall height). Other data-related uncertainties derive from the set-up of this study, where reference DTMs of VER-D and ROU-L were used for VER-O and ROU-P as well (in order to provide a more precise or complete reference). In this case, comparisons between produced and reference DTMs have a systematic error due to different data origins (two distinct photogrammetric analyses for VER-datasets, or laser altimetry vs. satellite stereography for ROU-datasets).

4.3 Potential applications

With the development of a robust, reliable and rapid tool for DTM generation from the DSM, studies related to feature detection and inventories can be facilitated. Particularly considering that (semi-)automatic feature extraction is typically sensitive for sharp terrain features and curvature (Bailly and Levavasseur, 2012; Sofia et al., 2016, 2014; Tarolli et al., 2014), the preservative performance TERRA algorithm is very suitable for this analysis, and carries strong potential for large-scale application. Apart from the focus on terraced landscapes, the algorithm might also perform well in landscapes with similar features, such as open-pit mines, riparian zones in anthropogenic lowlands (polders), or urban ramps (Sithole and Vosselman, 2004), provided that a sloping surface is present. Similarly, in such applications, it may become a powerful DTM preparation tool to aid feature extraction analyses, such as in the mapping of drainage networks (Bailly et al., 2008), landslide crowns (Tarolli et al., 2012), open-pit mines (Xiang et al., 2018), or for the geomorphometric characterisation of anthropogenic features (Tarolli et al., 2019). Finally, due to its ability to erase small obstacles along slopes, the proposed filter may also be beneficial for pre-processing noisy DEMs before hydrological analyses based on flow direction computing. Further research is needed and encouraged to explore the potential of the TERRA algorithm, and to test it as a pre-processing link in a longer chain of topographic analyses.

5. CONCLUSIONS

The proposed TERRA filtering algorithm is shown to have a convincing performance in first tests. Filtered DTMs produced from DSMs are relatively close to the reference DTMs in the six datasets, under various conditions of topography, presence of aboveground features, and data source and resolution. Sharp terrain features such as terrace edges are very well preserved (low Type I errors), which distinguishes the TERRA algorithm from most existing filters. Minor Type II errors occur where terrace edges are covered by vegetation on top of the terrace, or form a continuous surface with downslope vegetation located at the foot of the terrace wall.

Presented results create confidence for further application of the algorithm, based on its filtering skill and supported by minimal parameterisation requirements and computational efficiency due to the raster-based approach (as compared to a 3D-cloud-based approach). Further applications and analyses are encouraged for DTM creation and testing purposes. The algorithm may also play a key role in (semi-)automatic mapping of terrace structures, allowing a rapid DTM preparation step while maintaining typical terrain features (e.g. sharp edges) often critical for such analyses. Testing for DSM filtering in other environments such as anthropogenic landscapes with sloping terrain (e.g. hydraulic engineered lowlands, open-pit mines) is also encouraged in future exploration. The TERRA algorithm is freely available as R script under GNU GPL licence at: https://www.umr-lisah.fr/?q=fr/scriptsr/terra-script-r (see Supplementary Material A).

ACKNOWLEDGEMENTS

This work is part of the HighLandDEM project funded by the MISTRALS EnviMed IV program. It was partly supported by project ViTE “Vineyard Terraced landscapes: understanding the Environmental constraints to improve sustainable managements”, funded by the Linda Scattolin research program at TESAF department of the University of Padova (Italy). The authors would further like to thank data providers French Space Agency CNES and Airbus Defense and Space for Pleiades images, the Tunisian office of topography and cadastre for aerial images, the French National Program for Remote Sensing PTNS and the CNES R&T program for LiDAR data acquisition, and UAV-services *Zenith Aerial Solutions s.r.l* (October 2017 mission) and *Cambisol B.V.* (December 2017 mission) for drone-imagery.

REFERENCES

Axelsson, P., 1999. Processing of laser scanner data—algorithms and applications. ISPRS J. Photogramm. Remote Sens. 54, 138–147.

Bailly, J.S., Lagacherie, P., Millier, C., Puech, C., Kosuth, P., 2008. Agrarian landscapes linear features detection from LiDAR: Application to artificial drainage networks. Int. J. Remote Sens. 29, 3489–3508.

Bailly, J.S., Levavasseur, F., 2012. Potential of linear features detection in a Mediterranean landscape from 3D VHR optical data: application to terrace walls. In: Geoscience and Remote Sensing Symposium (IGARSS). pp. 7110–7113.

Brodu, N., Lague, D., 2012. 3D terrestrial lidar data classification of complex natural scenes using a multi-scale dimensionality criterion: Applications in geomorphology. ISPRS J. Photogramm. Remote Sens. 68, 121–134.

Brovelli, M.A., Cannata, M., Longoni, U.M., 2002. Managing and processing LIDAR data within GRASS. In: Proc. GRASS Users Conference. University of Trento, Italy, Trento, Italy, p. 29.

Burgos, S., Mota, M., Noll, D., Cannelle, B., 2015. Use of very high-resolution airborne images to analyse 3D canopy architecture of a vineyard. Int. Arch. Photogramm. Remote Sens. Spat. Inf. Sci. - ISPRS Arch. 40, 399–403.

Chen, Q., Gong, P., Baldocchi, D., Xie, G., 2007. Filtering Airborne Laser Scanning Data with Morphological Methods. Photogramm. Eng. Remote Sens. 73, 175–185.

Dela-Cruz, M.J., Koohafkan, P., 2009. Globally important agricultural heritage systems: a shared vision of agricultural, ecological and traditional societal sustainability. Resour. Sci. 31, 905–913.

Elmqvist, M., Jungert, E., Lantz, F., Persson, Å., U.Söderman, 2001. Terrain modelling and analysis using laser scanning data. Int. Arch. Photogramm. Remote Sens. XXXIV, 219–226.

Grilli, E., Menna, F., Remondino, F., 2017. A review of point clouds segmentation and classification algorithms. Int. Arch. Photogramm. Remote Sens. Spat. Inf. Sci. - ISPRS Arch. 42, 339–344.

He, Y., Zhang, C., Fraser, C.S., 2018. Progressive Filtering of Airborne LiDAR Point Clouds Using Graph Cuts. IEEE J. Sel. Top. Appl. Earth Obs. Remote Sens. 11, 2933–2944.

Kraus, K., Pfeifer, N., 1998. Determination of terrain models in wooded areas with airborne laser scanner data. ISPRS J. Photogramm. Remote Sens. 53, 193–203.

Lane, S.N., James, T.D., Crowell, M.D., 2000. Application of digital photogrammetry to complex topography for geomorphological research. Photogramm. Rec. 16, 793–821.

Lermé, N., Malgouyres, F., 2017. A Reduction Method For Graph Cut Optimization. Pattern Anal. Appl. 17, 361–378.

Liu, X., 2008. Airborne LiDAR for DEM generation: Some critical issues. Prog. Phys. Geogr. 32, 31–49.

Meng, X., Currit, N., Zhao, K., 2010. Ground filtering algorithms for airborne LiDAR data: A review of critical issues. Remote Sens. 2, 833–860.

Meng, X., Wang, L., Silván-Cárdenas, J.L., Currit, N., 2009. A multi-directional ground filtering algorithm for airborne LIDAR. ISPRS J. Photogramm. Remote Sens. 64, 117–124.

Molénat, J., Raclot, D., Zitouna, R., Andrieux, P., Coulouma, G., Feurer, D., Grunberger, O., Lamachère, J.M., Bailly, J.S., Belotti, J.L., Ben Azzez, K., Ben Mechlia, N., Ben Younès Louati, M., Biarnès, A., Blanca, Y., Carrière, D., Chaabane, H., Dagès, C., Debabria, A., Dubreuil, A., Fabre, J.C., Fages, D., Floure, C., Garnier, F., Geniez, C., Gomez, C., Hamdi, R., Huttel, O., Jacob, F., Jenhaoui, Z., Lagacherie, P., Le Bissonnais, Y., Louati, R., Louchart, X., Mekki, I., Moussa, R., Negro, S., Pépin, Y., Prévot, L., Samouelian, A., Seidel, J.L., Trotoux, G., Troiano, S., Vinatier, F., Zante, P., Zrelli, J., Albergel, J., Voltz, M., 2018. OMERE: A Long-Term Observatory of Soil and Water Resources, in Interaction with Agricultural and Land Management in Mediterranean Hilly Catchments. Vadose Zo. J. 17, 0.

Paroissien, J.-B., Lagacherie, P., Le Bissonnais, Y., 2010. A regional-scale study of multi-decennial erosion of vineyard fields using vine-stock unearthing–burying measurements. Catena 82, 159–168.

Passalacqua, P., Belmont, P., Staley, D.M., Simley, J.D., Arrowsmith, J.R., Bode, C.A., Crosby, C., DeLong, S.B., Glenn, N.F., Kelly, S.A., Lague, D., Sangireddy, H., Schaffrath, K., Tarboton, D.G., Wasklewicz, T., Wheaton, J.M., 2015. Analyzing high resolution topography for advancing the understanding of mass and energy transfer through landscapes: A review. Earth-Science Rev. 148, 174–193.

Perona, P., Malik, J., 1990. Scale-Space and Edge Detection Using Anisotropic Diffusion. IEEE Trans. Pattern Anal. Mach. Intell. 12, 629–639.

Pfeifer, N., Kostli, A., Kraus, K., 1998. Interpolation and filtering of laser scanner data—implementation and first results. Interpolat. Filter. laser scanner data—implementation first results XXXII, 153–159.

Pierrot-Deseilligny, M., De Luca, L., Remondino, F., 2011. Automated image-based procedures for accurate artifacts 3D modeling and orthoimage generation. Geoinf. FCE CTU 6, 291–299.

Pierrot-Deseilligny, M., Paparoditis, N., 2006. A multiresolution and optimization-based image matching approach: An application to surface reconstruction from spot5-hrs stereo imagery. In: Proceedings IAPRS. Ankara, Turkey, Turkey.

Pijl, A., Barneveld, P., Mauri, L., Borsato, E., Grigolato, S., Tarolli, P., 2019a. Impact of mechanisation on soil loss in terraced vineyard landscapes. Cuad. Investig. Geográfica 45, 287–308.

Pijl, A., Tosoni, M., Roder, G., Sofia, G., Tarolli, P., 2019b. Design of terrace drainage networks using UAV-based high-resolution topographic data. Water 11 (4), 814.

Pingel, T.J., Clarke, K.C., McBride, W.A., 2013. An improved simple morphological filter for the terrain classification of airborne LIDAR data. ISPRS J. Photogramm. Remote Sens. 77, 21–30.

Roggero, M., 2001. Airborne Laser Scanning: Clustering in Raw Data. ISPRS J. Photogramm. Remote Sens. XXXIV, 227–232.

Santesteban, L.G., Guillaume, S., Royo, J.B., Tisseyre, B., 2013. Are precision agriculture tools and methods relevant at the whole-vineyard scale? Precis. Agric. 14, 2–17.

Shan, J., Aparajithan, S., 2005. Urban DEM Generation from Raw Lidar Data. Photogramm. Eng. Remote Sens. 71, 217–226.

Sithole, G., 2001. Filtering of laser altimetry data using a slope adaptive filter. Int. Arch. Photogramm. Remote Sens. Spat. Inf. Sci. XXXIV, 203– 210.

Sithole, G., Vosselman, G., 2004. Experimental comparison of filter algorithms for bare-Earth extraction from airborne laser scanning point clouds. ISPRS J. Photogramm. Remote Sens. 59, 85–101.

Sofia, G., Bailly, J.S., Chehata, N., Tarolli, P., Levavasseur, F., 2016. Comparison of Pleiades and LiDAR Digital Elevation Models for Terraces Detection in Farmlands. IEEE J. Sel. Top. Appl. Earth Obs. Remote Sens. 9, 1567–1576.

Sofia, G., Marinello, F., Tarolli, P., 2014. A new landscape metric for the identification of terraced sites: The Slope Local Length of Auto-Correlation (SLLAC). ISPRS J. Photogramm. Remote Sens. 96, 123–133.

Sohn, G., Dowman, I., 2002. Terrain surface reconstruction by the use of tethrahedron model with the MDL criterion. Int. Arch. Photogramm. Remote Sens. Spat. Inf. Sci. XXXIV, 336–344.

Tarolli, P., 2014. High-resolution topography for understanding Earth surface processes: Opportunities and challenges. Geomorphology 216, 295–312.

Tarolli, P., Cao, W., Sofia, G., Evans, D., Ellis, E.C., 2019. From features to fingerprints: A general diagnostic framework for anthropogenic geomorphology. Prog. Phys. Geogr. 43, 95–128.

Tarolli, P., Preti, F., Romano, N., 2014. Terraced landscapes: From an old best practice to a potential hazard for soil degradation due to land abandonment. Anthropocene 6, 10–25.

Tarolli, P., Sofia, G., Calligaro, S., Prosdocimi, M., Preti, F., Dalla Fontana, G., 2015. Vineyards in terraced landscapes: new opportunities from lidar data. L. Degrad. Dev. 26, 92–102.

Tarolli, P., Sofia, G., Dalla Fontana, G., 2012. Geomorphic features extraction from high-resolution topography: Landslide crowns and bank erosion. Nat. Hazards 61, 65–83.

Ural, S., Shan, J., 2016. A min-cut based filter for airborne Lidar data. Int. Arch. Photogramm. Remote Sens. Spat. Inf. Sci. - ISPRS Arch. 41, 395–401.

Vosselman, G., 2000. Slope based filtering of laser alitmetry data. Int. Arch. Photogramm. Remote Sens. XXXIII, 935–942.

Wack, R., Wimmer, A., 2002. Digital terrain models from airborne laser scanner data – a grid based approach. Int. Arch. Photogramm. Remote Sens. Spat. Inf. Sci. XXXIV, 293–296.

Wei, W., Chen, D., Wang, L., Daryanto, S., Chen, L., Yu, Y., Lu, Y., Sun, G., Feng, T., 2016. Global synthesis of the classifications, distributions, benefits and issues of terracing. Earth-Science Rev. 159, 388–403.

Xiang, J., Chen, J., Sofia, G., Tian, Y., Tarolli, P., 2018. Open-pit mine geomorphic changes analysis using multi-temporal UAV survey. Environ. Earth Sci. 77, 1–18.

Yang, B., Huang, R., Dong, Z., Zang, Y., Li, J., 2016. ISPRS Journal of Photogrammetry and Remote Sensing Two-step adaptive extraction method for ground points and breaklines from lidar point clouds. ISPRS J. Photogramm. Remote Sens. 119, 373–389.

Zhang, K., Chen, S.-C., Whitman, D., Shyu, M.-L., Yan, J., Zhang, C., 2003. A Progressive Morphological Filter for Removing Nonground Measurements From Airborne LIDAR Data. IEEE Trans. Geosci. Remote Sens. 41, 872–882.

SUPPLEMENTARY MATERIAL A: R script TERRA

```
################################################################################
## available at https://www.umr-lisah.fr/?q=fr/scriptsr/terra-script-r
################################################################################

################################################################################
#  This file is the R code of the TERRA algorithm
#  see
#  https://doi.org/10.1016/j.jag.2019.101977
#  "TERRA: Terrain extraction from elevation rasters through repetitive
#  anisotropic filtering#
#  Copyright(c) 2019, AgroParisTech
#  == GNU General Public License Usage ==
#  TERRA.R is a free tool: you can redistribute it and/or modify
#  it under the terms of the GNU General Public License as published by
#  the Free Software Foundation, either version 3 of the License, or
#  (at your option) any later version.
#  TERRA.R is distributed in the hope that it will be useful,
#  but WITHOUT ANY WARRANTY; without even the implied warranty of
#  MERCHANTABILITY or FITNESS FOR A PARTICULAR PURPOSE.  See the
#  GNU General Public License for more details.
#  See <http://www.gnu.org/licenses/>
#  == Other Usage ==
#  Other Usage means a use of TERRA algorithm that is inconsistent with the GPL
#  license, and requires a written agreement between You and AgroParisTech.
#  Licensees for Other Usage of TERRA.R may use this file in accordance
#  with the terms contained in the written agreement between You and AgroParisTech.
################################################################################


################################################################################
#  @author Jean-Stéphane BAILLY <bailly@agroparistech.fr>
################################################################################


################################################################################
#  Require to call first the "raster" R package
################################################################################


################################################################################
# Input and parameters
# Input :
# - dsm : dsm name to be filtered in raster R format
# Parameters :
# - lambda : Kernel size
# - eta : spatial aggregation factor
# - M : number of iteration
################################################################################

################################################################################
#  Output :
#  - filtered dtm in raster R format
################################################################################

################################################################################
#  Note that the Kernel statistic used here is the mean but it can be changed
#  manually by any other statistics (min, median, etc)
################################################################################

################################################################################
#  Execution example including TERRA compilation :
#  source('TERRA.R')
#  mnt<-TERRA(dsm=mns,lambda=7,eta=10, M=5)
```

```
#############################################################################

TERRA<-function(dsm=mns,lambda=7,eta=10, M=5)
{

#structural element inner aspect
K<-matrix(0,lambda,lambda)
X<-col(K)-(((lambda-1)/2))-1
Y<-(nrow(K)-row(K))-((lambda-1)/2)
azi<-atan(Y/X)
azi[X<0]<-azi[X<0]+pi
azi[X>=0 & Y<0]<-azi[X>=0 & Y<0]+2*pi
azi<-2*pi-azi
azi[azi==(2*pi)]<-0
azi<-azi+(pi/2)
azi[azi>=(2*pi) & !is.nan(azi)]<-azi[azi>=(2*pi) & !is.nan(azi)]-(2*pi)


DSM<-dsm

for(i in 1:M)
{

#low frequency slope calculation
AGG<-aggregate(DSM, fact=eta, expand=TRUE)
ASP<-terrain(AGG, opt='aspect', unit='radians')
asp<-resample(ASP, DSM, method="ngb")
MNS<-as.matrix(DSM)
ASP<-as.matrix(asp)


MNT<-MNS
for (i in (1+(lambda-1)/2):(nrow(MNS)-(lambda-1)/2))   # i: row.index
{
       for (j in (1+(lambda-1)/2):(ncol(MNS)-(lambda-1)/2))   # j: col.index
       {
              if(!is.na(ASP[i,j]))
              {
                     shift<-ASP[i,j]
                     s1<-azi>=(shift-pi/2) | azi>=(shift+3*pi/2) | azi<=(shift-3*pi/2)
                     s2<-azi<=(shift+pi/2) | azi>=(shift+3*pi/2) | azi<=(shift-3*pi/2)
                     W<-(s1 & s2)
                     W[((lambda-1)/2)+1,((lambda-1)/2)+1]<-TRUE
                     W<-!(W)
                     cand<-mean((W*MNS[(i-((lambda-1)/2)):(i+((lambda-1)/2)),(j-((lambda-
1)/2)):(j+((lambda-1)/2))])[W==T], na.rm=T)
                     if(!is.na(cand)){ if(cand<MNT[i,j]) {MNT[i,j]<-cand}}
              }
       }
}
values(DSM)<-MNT
}
mnt<-dsm
values(mnt)<-MNT
invisible(return(mnt))
}
```